PCCP

Accepted Manuscript

ROYAL SOCIETY OF CHEMISTRY

www.rsc.org/pccp

Journal Name

RSCPublishing

ARTICLE

Negative Thermal Quenching of Photoluminescence in Annealed ZnO/Al_2O_3 Core/Shell Nanorods

Cite this: DOI: 10.1039/x0xx00000x

Yukun Wu[a], Junwen Li[a], Huaiyi Ding[b], Zhiwei Gao[a], Yiming Wu[a], Nan Pan[b] and Xiaoping Wang[a,b*]

Received 00th January 2012,
Accepted 00th January 2012

DOI: 10.1039/x0xx00000x

www.rsc.org/

ZnO/Al_2O_3 core/shell nanorods (NRs) have been fabricated through vapor phase condensation method and atomic layer deposition. It is found that the nanorod comprises a wurtzite single crystal ZnO core with the main axes along [0001] direction and an amorphous Al_2O_3 shell. The temperature-dependent photoluminescence (PL) properties of as-grown and annealed ZnO/Al_2O_3 NRs are investigated systematically. The PL of as-grown ZnO/Al_2O_3 NRs demonstrates normal thermal quenching feature. However, the salient behavior of negative thermal quenching (NTQ), i.e., the PL intensity increases with increasing temperature, is clearly observed in the annealed ZnO/Al_2O_3 NRs. A multi-level model is adopted to account for this behavior and the thermal activation energy for NTQ process is estimated of ~69 meV. Moreover, we suggest that the activation energy is related to the Al donor defect in ZnO resulted from the inter-diffusion between ZnO core and Al_2O_3 shell during the annealing process.

Introduction

As a wide direct band gap semiconductor, ZnO nanostructure has a broad range of potential applications for nanoelectronic and optoelectronic devices, such as transistors[1, 2], diodes[3], lasing[4, 5], hybrid solar cells[6], photodetectors[7-10], sensors[11-13], and among others. Due to its high surface-to-volume ratio, the optical properties of ZnO nanostructure depend critically on the surface structure as well as the defects in the material[14-16]. In this context, a variety of surface passivation and defect engineering methods are proposed to modulate its optical properties. Atomic layer deposition (ALD), with the unique advantages of precise thickness control and conformal deposition, has been widely applied as an important surface modification method to this end[17-21]. For example, several previous studies have demonstrated that the optical properties of ZnO nanostructures can be tuned by ALD coating[22-26]. As to improve the interface between the nanostructure and ALD coating, the annealing process is often adopted to enhance the performance of the nanostructures. The PL of ZnO/Al_2O_3 nanorods (NRs) has been reported to show a significant enhancement after thermal annealing[24]. On the other hand, the annealing process might inevitably induce unintentional donors and produce intermediate states in the semiconductors. It has been pointed out that the intermediate states can affect the PL transition of excitons to a certain extent and lead to an abnormal negative thermal quenching (NTQ) behavior occasionally, in which the PL intensity of the nanostructure increases with increasing temperature under certain temperature range. So far, even NTQ has been observed in some materials including GaAs, ZnS and ZnO[27-31], there is no report for ZnO/Al_2O_3 core/shell NRs.

In this work, we prepared ZnO/Al_2O_3 NRs through vapor phase condensation (VPC) method and atomic layer deposition. Various characterizations have been performed and the results reveal that the ZnO core is wurtzite single crystal with the main axes along [0001] direction and the Al_2O_3 shell is amorphous. The temperature-dependent PL measurement is carried out to investigate the annealing effect on the optical properties of ZnO/Al_2O_3 NRs. It is found that, although the PL of as-grown ZnO/Al_2O_3 NRs shows a normal thermal quenching feature, the NTQ phenomenon can be clearly observed in the annealed ZnO/Al_2O_3 NRs. Based on a multi-level model proposed by Shibata[32], the thermal activation energy of ~69 meV accounted for NTQ is obtained. We suggest that the activation energy is related to the Al donor defect in ZnO resulted from the inter-diffusion between ZnO core and Al_2O_3 shell during the annealing process. The result can further enrich our knowledge of the defect effect on the optical properties of ZnO nanostructure.

Experimental section

The ZnO NRs were prepared by the VPC method in a two-heating-zone tube furnace. Details can be found elsewhere[14]. Briefly, high-purity ZnO powder and spectrograde graphite powder at a molar ratio of 1:1 were mixed uniformly as the precursor, and Si (111) wafers covered with a 500 nm-thick ZnO seed-layer were used as the growth substrates. During growth, the source temperature was kept at 1000 °C while the substrate temperature maintained at 650 °C. Ar (10 SCCM) and O_2 (9 SCCM) were used as the carrier and reactive gas, respectively, and the growth time was 15 minutes. ZnO/Al_2O_3 NRs were fabricated through coating ZnO NRs with a thin

Al_2O_3 layer by ALD. In the ALD process, trimethylaluminum (TMA) and water were employed as the precursors, and the reaction was carried out at 200 °C with N_2 as the carrier gas. The annealed ZnO NRs and annealed ZnO/Al_2O_3 NRs were obtained through annealing as-grown ZnO NRs and as-grown ZnO/Al_2O_3 NRs in air at 500 °C for 1 hour.

The morphologies and structures of the various NRs were characterized by field-emission scanning electron microscopy (FE-SEM, JEOL-6700) and transmission electron microscopy (TEM, JEOL-2010), sequentially. The crystallinities of the samples were investigated by X-ray diffraction (XRD, Rigaku TTR-III X-ray diffractometer) with Cu *Kα* line. Room Temperature PL (RT-PL) and variable-temperature PL (VT-PL) properties of the samples were measured under 325 nm excitation using LabRAM HR 800 and Fluorolog Tau-3 Lifetime System, Horiba Jobin Yvon Inc. During the VT-PL measurement, the solid sample was fixed in a cooling stage, which can be cooled down to ~9K by a closed cycle refrigerator. All the photoluminescence measurements were carried out on pristine ZnO and ZnO/Al_2O_3 NR arrays from 9K till room temperature.

Results and discussion

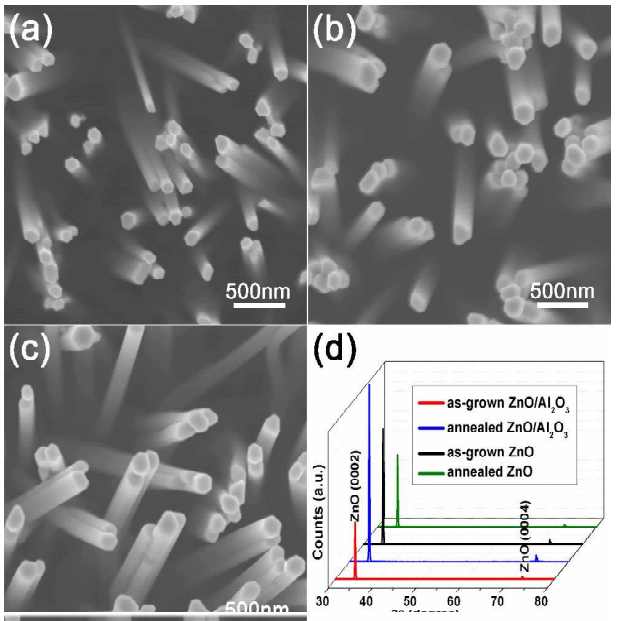

Figure 1. SEM images of (a) as-grown ZnO NRs, (b) as-grown ZnO/Al_2O_3 NRs and (c) annealed ZnO/Al_2O_3 NR, respectively. (d) XRD patterns of different samples.

Figure 1(a-c) show SEM images of as-grown ZnO NRs, ZnO/Al_2O_3 NRs and annealed ZnO/Al_2O_3 NRs, respectively. As seen, the diameter of as-grown NRs is about 90 ~150 nm while the length is between 7 ~10μm (measured from the side view SEM images in Figure S1). After coated with a thin Al_2O_3 layer by ALD, the diameter increases to 140 ~ 230 nm, implying the thickness of the Al_2O_3 shell ~25nm. Moreover, we find that all NRs have similar morphologies, suggesting neither coating nor annealing treatment can alter the morphologies of the NRs. The XRD results of various NRs are shown in Figure 1d. As seen, all samples demonstrate only two diffraction peaks corresponding to (0002) and (0004) ZnO planes, indicating all NRs possess good wurtzite single crystal structure.

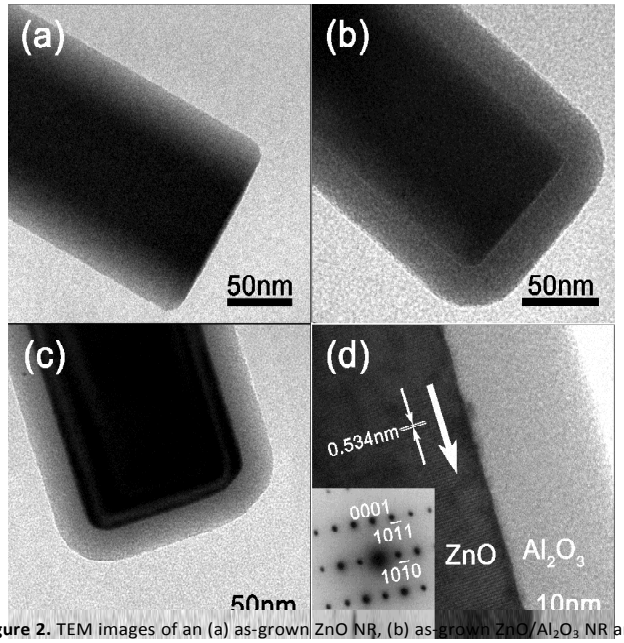

Figure 2. TEM images of an (a) as-grown ZnO NR, (b) as-grown ZnO/Al_2O_3 NR and (c) annealed ZnO/Al_2O_3 NR, respectively. (d) HRTEM image of the annealed ZnO/Al_2O_3 NR with the SEAD patterns shown in the inset.

TEM images of various NRs are revealed in Figure 2 (a-c), from which the good interface can be observed between ZnO core and Al_2O_3 shell. Moreover, the thickness of Al_2O_3 shell is estimated to be 25nm, in agreement with the result of SEM (Figure 1b and 1c). Figure 2d is the high resolution TEM (HRTEM) image of the annealed ZnO/Al_2O_3 NR and the HRTEM results for the as-grown ZnO NR and as-grown ZnO/Al_2O_3 NR can be found in figure S2. It is clear seen that the ZnO core is wurtzite single crystalline with the main axes along [0001] direction (indicated by the white arrow), while the Al_2O_3 shell is amorphous. Additionally, the selected area electron diffraction (SEAD) result shown in the inset of Figure 2d also displays only ZnO wurtzite patterns. Both of the clear lattice of (0001) plane of ZnO and the bright diffraction spots imply that the good crystal quality of NRs can be preserved even after annealing.

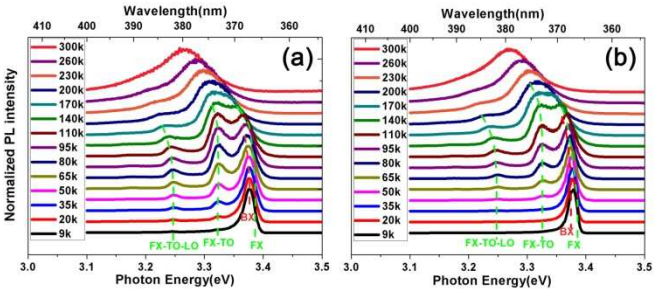

Figure 3. Variable-temperature PL spectra of (a) as-grown and (b) annealed ZnO/Al_2O_3 NRs. Bound exciton (BX), free exciton (FX) and its phonon replicas can be distinguished clearly. The spectra are normalized and shifted for clarity.

PL properties of different NR samples are further investigated. Figure 3 shows the VT-PL results of as-grown and annealed ZnO/Al_2O_3 NRs from 8K to 300 K. As seen, two samples possess similar behavior. The peaks of bound exciton (BX), free exciton (FX) and its corresponding phonon replicas are clearly identified and labeled on the spectra. A dominant asymmetric peak at ~3.373 eV at low temperature can be assigned to the contributions from ionized donor BX (3.367 eV, red dash line) and FX (3.377 eV) of ZnO. The transverse-optical (TO) and longitudinal-optical (LO) phonon replicas of FX are also observed, with the peak position at ~3.296 eV and ~3.226 eV, respectively. As the temperature increases, the FX emission as well as its phonon replicas (indicated by the green dash lines in Figure 3) increases. This is because more thermally activated BXs convert to FXs. By comparing the spectrum of as-grown ZnO/Al_2O_3 NRs carefully with that of the annealed sample, we find that the relative intensity ratio of phonon replicas to the FX and BX from the as-grown sample is obviously larger than that from the annealed sample. This behavior is readily observed in the temperature range of 30 K ~ 110 K. The result indicates that the electron-phonon coupling (EPC) in ZnO core, which can be affected by the nonstoichiometry and the defects[14], is rather different in both samples.

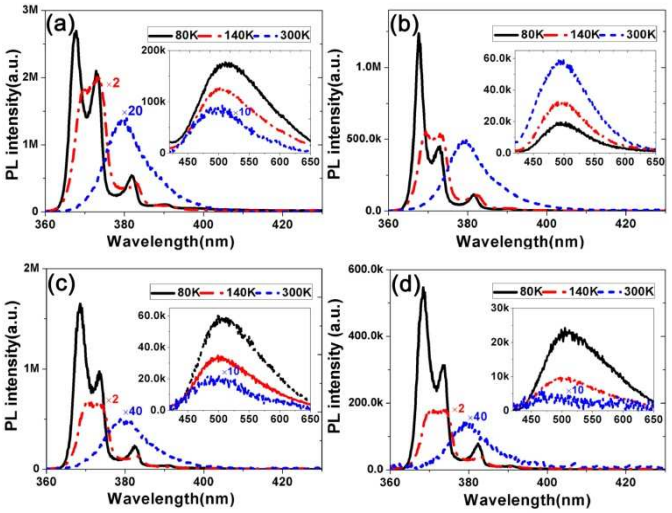

Figure 4. NBE and DL (insets) emissions of different samples measured at 80K, 140K and 300K. (a) as-grown ZnO/Al_2O_3 NRs, (b) annealed ZnO/Al_2O_3 NRs, (c) as-grown ZnO NRs and (d) annealed ZnO NRs.

Remarkably, we find that the photoluminescence intensity of the annealed ZnO/Al_2O_3 NRs demonstrates different temperature dependency as compared to that of the as-grown one. Figure 4a and 4b show typical results of the samples measured at 80 K, 140 K and room temperature (RT), respectively. As seen, the intensity of near band edge (NBE) emission from as-grown sample decreases dramatically with increasing temperature. For example, the intensity measured at RT is at least twenty times less than that at 140K. On the contrary, the PL intensity for the annealed ZnO/Al_2O_3 NRs at RT is almost the same as that at 140K. In addition, the variations of intensity of deep level (DL) emission ranging from 420 nm to 650 nm with the temperature are also displayed in the inset of Figure 4(a-b) (note that the DL spectra is obtained simultaneously with the NBE spectra under 325 nm excitation). It can be found that the intensity of DL emission for as-grown sample decreases with temperature, while that for the annealed one shows substantially an opposite tendency. Clearly, the DL intensity from the annealed ZnO/Al_2O_3 NRs at RT is 3 times as large as that at 80K. In order to understand whether the behavior is particularly related to the annealed ZnO/Al_2O_3 NRs, we performed the same measurements on the as-grown ZnO NRs and annealed ZnO NRs. As seen from Figure 4c and 4d, we find that both ZnO NRs samples show the same temperature dependence of PL intensity as that observed in the as-grown ZnO/Al_2O_3 NRs (Figure 4a), i.e., the PL intensities decay very rapidly from 80K to RT. The results accord well with the general expectation of thermal quenching of photoluminescence with increasing temperature.

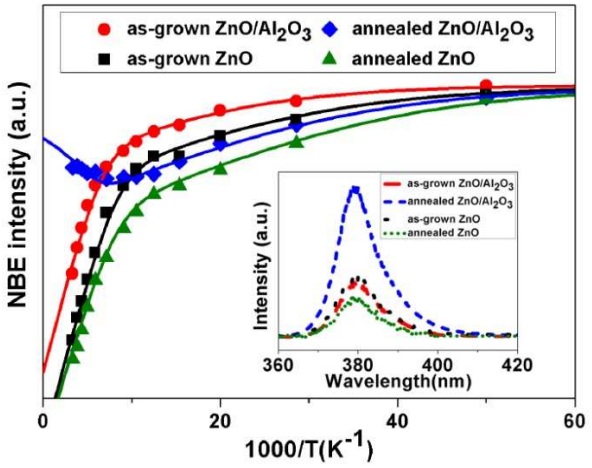

Figure 5. The integrated intensity of NBE emission in the range of 360-400nm as a function of temperature for the as-grown ZnO/Al_2O_3 NRs, annealed ZnO/Al_2O_3 NRs, as-grown ZnO NRs and annealed ZnO NRs. The solid lines are the fitting curves using Eq. (1). Inset shows the room temperature PL spectra of four different samples.

In order to examine the variation of PL intensities with temperature clearly, the integrated intensities of NBE emission of various samples in the range of 360-400nm are plotted in Figure 5. The intensities of DL emission from 420-650nm can be found in Figure S4. For the as-grown ZnO NRs, annealed ZnO NRs and as-grown ZnO/Al_2O_3 NRs, the intensities of NBE emission all decrease monotonically with increasing temperature, and the intensities of DL emission vary steadily from 20K to 80K then drop dramatically to RT. For the annealed ZnO/Al_2O_3 NRs, in low temperature range (20K-80K), the NBE and DL intensities show similar temperature dependencies to those observed in other samples, respectively. However, they become increasing apparently with the temperature from 140K up to RT. This behavior is designated as a negative thermal quenching (NTQ). It should be emphasized that the NTQ behavior is particular to the annealed ZnO/Al_2O_3 NRs in our study. For clarity, in the inset of Figure 5, we also demonstrate the PL spectra of four samples at RT, from which the NBE intensity of the annealed ZnO/Al_2O_3 NRs is observed manifestly much stronger than those of other samples. It should be pointed out that the variation of PL intensities for different samples cannot be attributed to either the diversity of the density of NRs or the changes of the

absorption properties. In fact, four ZnO NRs samples in this study come from the same batch of fabrication processing, and their morphologies and densities of NRs are similar as observed in SEM images. Moreover, the absorption spectra of NRs are also performed, and as seen in figure S3, the results show that four kinds of samples possess nearly the same intensity and absorption edge at ~390 nm.

To investigate the origination of NTQ behavior, we first retrospect to the morphological and structural characteristics. As in aforementioned discussion, considering that all samples show similar morphology and good crystal quality (Figure 1, 2 and S2), their contributions to NTQ can be safely excluded. On the other hand, although a good interface is observed from the HRTEM image of the annealed ZnO/Al_2O_3 NR, several small fuzzy regions can yet be found from Figure 2d in the core area. This is contrast to the case of as-grown ZnO/Al_2O_3 NR, where no such region can be found (Figure S2b). Earlier work[33-35] has revealed that the Kirkendall effect can occur in ZnO/Al_2O_3 core/shell nanowires annealed above 700 °C. At moderate annealing temperature, such as 500 °C in our experiments, it has also been reported that the inter-diffusion between core and shell can happen[36]. Hence, we consider that the fuzzy regions are possibly originated from the inter-diffusion between ZnO and Al_2O_3, and as a result, the inter-diffusion can also induce Al donor defects in the ZnO core.

It has been pointed out that the variation of PL intensity with the temperature I(T) can be described by a multi-level model developed by Shibata[32], which is expressed as

$$I(T) = I(0)\frac{1+\sum_{q=1}^{w} D_q \exp(-E'_q / k_B T)}{1+\sum_{j=1}^{m} C_j \exp(-E_j / k_B T)} \quad (1)$$

where k_B is the Boltzmann constant, T is the temperature, E_j (E'_q) describes the activation energy for the process that decreases (increases) of the PL intensity with the temperature, and C_j (D_q) is the corresponding weight factor. In this equation, the exponential item in the denominator is related to the normal temperature quenching process, while the exponential item in the numerator can be used to describe the NTQ process. The experimental data are fitted by this equation and the fitting results are plotted with curves in Figure 5. The fitted activation energies for different samples are also summarized in Table 1. As seen, the fitting results agree excellently with the experimental data, indicating the model is well appropriate to depict the variation of photoluminescence with the temperature. For as-grown ZnO NRs, annealed ZnO NRs and as-grown ZnO/Al_2O_3 NRs, there only exists normal thermal quenching for all the NBE and DL emission process, and two activation energies of E_1 in the range of 54~63 meV and E_2 in the range of 7~8 meV can be estimated. Considering that the energy difference between BX (3.367eV) and FX (3.377eV) is about 10meV (Figure 3), we attribute E_2 to the thermal activation process for the conversion of BXs to FXs, which occurs frequently in the low temperature range. On the other hand, due to E_1 very close to the exciton binding energy of ZnO ~60 meV, we ascribe it to the thermal activation process for the exciton dissolution, which happens dominantly in the high temperature range. It is worth mentioning that, as the temperature increases, both processes can lower the radiative quantum efficiency of the excitons, resulting in the normal thermal quenching of photoluminescence.

Table 1. The activation energies deduced from the fitting in Figure 5 and S4 by Eq. (1).

	NBE			DL	
	E_1 (meV)	E_2 (meV)	E_1' (meV)	E_1 (meV)	E_1' (meV)
as-grown ZnO/Al_2O_3 NRs	62 ± 4	8 ± 2	-	63 ± 4	-
annealed ZnO/Al_2O_3 NRs	60 ± 2	7 ± 2	69 ± 2	63 ± 4	65 ± 3
as-grown ZnO NRs	60 ± 2	7 ± 2	-	60 ± 2	-
annealed ZnO NRs	55 ± 3	7 ± 1	-	54 ± 3	-

As to the annealed ZnO/Al_2O_3 NRs, apart from the activation energies of E_1 ~ 60 meV and E_2 ~ 7 meV, another activation energy of E_1' ~ 69 meV has to be included to fit the experimental data well in the whole temperature range. Similar to the aforementioned discussion, while E_1 and E_2 can be considered to relate to the normal thermal quenching process, E_1' is believed to correlate to the NTQ process. The origination of the activation energy for NTQ behavior has been suggested to come from the extrinsic defects in ZnO[37]. Due to the fact that there exists inter-diffusion during annealing the ZnO/Al_2O_3 NRs, we believe that the Al donor atoms in ZnO can act as the extrinsic defects to produce the NTQ behavior. The existed Al donor defects in the annealed ZnO/Al_2O_3 NRs can also be account for the difference EPC strength observed in as-grown and annealed ZnO/Al_2O_3 NRs (Figure 3). Moreover, the NBE emission of the annealed ZnO/Al_2O_3 NRs is observed to have a slight blue shift (~ 9 meV) as compared to that of the as-grown ZnO/Al_2O_3 NRs (Figure 3), and the intensity of green emission from the annealed ZnO/Al_2O_3 NRs is also higher than that from the as-grown one (inset in Figure S4). Both behaviors are consistent with the results of Al doped ZnO nanostructures reported by Fang *et al.*[38] Notably, our finding activation energy of ~ 69 meV for the annealed ZnO/Al_2O_3 NRs is also consistent with the data of previous reports. For example, Meyer *et al.*[39] and He *et al.*[40] have reported an activation energy of ~52 meV and 87 meV for Al donor in ZnO, respectively. Hur *et al.*[41] revealed an Al relevant localized level located at ~80 meV below the effective band edge of ZnO. To further understand whether the deep level luminescence comes from different defect centers, we investigate the photoluminescence excitation spectra (PLE) of different samples as well and the results are shown in Figure S5. It can be found that all PLE spectra vary smoothly, and both NBE and DL emissions of four samples can only be excited by UV light with wavelength shorter than 380 nm, implying that the deep level luminescence of the sample does not result from different centers.

Though the main purpose of this paper is to report the observed NTQ behavior in the annealed ZnO/Al_2O_3 NRs, below we provide a plausible explanation. Under excitation with 325 nm light, the photon-generated excitons can either act as BXs and

FXs in the ZnO or be trapped by the Al donors. For the as-grown ZnO/Al_2O_3 NRs, BXs can convert to FXs in the low temperature range, and FXs further become broken in higher temperature range through overcoming the binding energy of 60 meV, leading to the drop of photoluminescence intensity with increasing temperature. The processes are corresponding to the normal thermal quenching behavior. For the annealed ZnO/Al_2O_3 NRs, however, in the high temperature range above 140 K, the Al trapped excitons can be released gradually by the thermal active process. This can raise the concentration of FXs and result in the increase of photoluminescence, leading to the NTQ behavior. Note that, even the exact underlying reason for the activation energy of E_1' remains unclear at the moment, the above interpretation, though tentative, provides a qualitative understanding of the observed NTQ phenomena for the annealed ZnO/Al_2O_3 NRs. More experimentation is needed to ascertain the exact origin of the activation energy of E_1' in the future.

Conclusions

We have synthesized ZnO/Al_2O_3 core/shell NRs through vapor phase condensation method and atomic layer deposition. The nanostructure comprises a wurtzite single crystal ZnO core and an amorphous Al_2O_3 shell. The temperature-dependent photoluminescence investigation is carried out systematically for the as-grown and annealed ZnO/Al_2O_3 NRs. While the as-grown ZnO/Al_2O_3 NRs show normal thermal quenching of PL, the annealed sample demonstrates distinct NTQ behavior. The results are well interpreted by a multi-level model through introducing a donor state with the thermal activation energy of ~69 meV. The thermal activation energy is attributed to the Al donor defects resulted from the inter-diffusion between ZnO core and Al_2O_3 shell during the annealing process. The finding can enrich our knowledge of the defect effect on the optical properties of ZnO nanostructure.

Acknowledgements

The authors acknowledge the financial support from MOST of China (2011CB921403), NSFC (11374274, 11074231) as well as by CAS (XDB01020000).

Notes and references

[a] Department of Physics, University of Science and Technology of China, Hefei, 230026, P. R. China.

[b] Hefei National Laboratory for Physical Sciences at the Microscale, University of Science and Technology of China, Hefei, 230026, P. R. China.

* Corresponding author E-mail: xpwang@ustc.edu.cn

† Electronic Supplementary Information (ESI) available: [details of any supplementary information available should be included here]. See DOI: 10.1039/b000000x/

1. P. C. Chang, Z. Fan, C. J. Chien, D. Stichtenoth, C. Ronning and J. G. Lu, *Appl Phys Lett*, 2006, **89**, 133113.
2. D. Kälblein, R. T. Weitz, H. J. Böttcher, F. Ante, U. Zschieschang, K. Kern and H. Klauk, *Nano Letters*, 2011, **11**, 5309-5315.
3. B. Ryu, Y. T. Lee, K. H. Lee, R. Ha, J. H. Park, H.-J. Choi and S. Im, *Nano Letters*, 2011, **11**, 4246-4250.
4. X. Huan-Ming, *Journal of Materials Chemistry*, 2010, **20**, 4251-4262.
5. A. Stassinopoulos, R. N. Das, E. P. Giannelis, S. H. Anastasiadis and D. Anglos, *Applied Surface Science*, 2005, **247**, 18-24.
6. G. Zhang, S. Jiang, Y. Lin, W. Ren, H. Cai, Y. Wu, Q. Zhang, N. Pan, Y. Luo and X. Wang, *Journal of Materials Chemistry A*, 2014, **2**, 5675-5681.
7. R. S. Aga, D. Jowhar, A. Ueda, Z. Pan, W. E. Collins, R. Mu, K. D. Singer and J. Shen, *Appl Phys Lett*, 2007, **91**, 232108.
8. W. Park, G. Jo, W. K. Hong, J. Yoon, M. Choe, S. Lee, Y. Ji, G. Kim, Y. H. Kahng, K. Lee, D. Wang and T. Lee, *Nanotechnology*, 2011, **22**, 205204.
9. C. Lao, Y. Li, C. P. Wong and Z. L. Wang, *Nano Letters*, 2007, **7**, 1323-1328.
10. L. Hu, J. Yan, M. Liao, H. Xiang, X. Gong, L. Zhang and X. Fang, *Advanced Materials*, 2012, **24**, 2305-2309.
11. M. Villani, D. Calestani, L. Lazzarini, L. Zanotti, R. Mosca and A. Zappettini, *Journal of Materials Chemistry*, 2012, **22**, 5694-5699.
12. Y. Zhang, Q. Xiang, J. Xu, P. Xu, Q. Pan and F. Li, *Journal of Materials Chemistry*, 2009, **19**, 4701-4706.
13. A. Joshi, D. K. Aswal, S. K. Gupta, J. V. Yakhmi and S. A. Gangal, *Appl Phys Lett*, 2009, **94**, 103115.
14. H. Y. Ding, Z. Zhao, G. H. Zhang, Y. K. Wu, Z. W. Gao, J. W. Li, K. Zhang, N. Pan and X. P. Wang, *J Phys Chem C*, 2012, **116**, 17294-17299.
15. H. Y. Ding, N. Pan, C. Ma, Y. K. Wu, J. W. Li, H. B. Cai, K. Zhang, G. H. Zhang, W. Z. Ren, J. Q. Li, Y. Luo, X. P. Wang and J. G. Hou, *Advanced Materials*, 2014, **26**, 3035-3041.
16. H. B. Zeng, G. T. Duan, Y. Li, S. K. Yang, X. X. Xu and W. P. Cai, *Advanced Functional Materials*, 2010, **20**, 561-572.
17. S. M. George, *Chem Rev*, 2010, **110**, 111-131.
18. M. Knez, K. Niesch and L. Niinisto, *Advanced Materials*, 2007, **19**, 3425-3438.
19. H. Kim, H.-B.-R. Lee and W. J. Maeng, *Thin Solid Films*, 2009, **517**, 2563-2580.
20. M. N. Liu, X. L. Li, S. K. Karuturi, A. I. Y. Tok and H. J. Fan, *Nanoscale*, 2012, **4**, 1522-1528.
21. C. Marichy, M. Bechelany and N. Pinna, *Advanced Materials*, 2012, **24**, 1017-1032.
22. W.-C. Sun, Y.-C. Yeh, C.-T. Ko, H. He, Jr. and M.-J. Chen, *Nanoscale Res. Lett.*, 2011, **6**, 556.
23. D. Zhao, X. Zhang, H. Dong, L. Yang, Q. Zeng, J. Li, L. Cai, X. Zhang, P. Luan, Q. Zhang, M. Tu, S. Wang, W. Zhou and S. Xie, *Nanoscale*, 2013, **5**, 4443-4448.
24. H. G. Cha, D. I. Kang, T. H. Kwon and Y. S. Kang, *Crystengcomm*, 2012, **14**, 1205-1209.
25. C. Chen, H. P. He, Y. F. Lu, K. W. Wu and Z. Z. Ye, *Acs Applied Materials & Interfaces*, 2013, **5**, 6354-6359.
26. M. A. Thomas and J. B. Cui, *Journal of Vacuum Science & Technology A*, 2012, **30**, 01A116.
27. E. H. Bogardus and H. B. Bebb, *Physical Review*, 1968, **176**, 993-&.
28. T. Yokogawa, T. Taguchi, S. Fujita and M. Satoh, *Ieee Transactions on Electron Devices*, 1983, **30**, 271-277.
29. M. Hauser, A. Hepting, R. Hauschild, H. Zhou, J. Fallert, H. Kalt and C. Klingshirn, *Appl Phys Lett*, 2008, **92**, 211105.
30. H. He, Z. Ye, S. Lin, B. Zhao, J. Huang and H. Tang, *J Phys Chem C*, 2008, **112**, 14262-14265.
31. X. H. Huang, C. Zhang, C. B. Tay, T. Venkatesan and S. J. Chua, *Appl Phys Lett*, 2013, **102**, 111106.
32. H. Shibata, *Japanese Journal of Applied Physics*, 1998, **37**, 550-553.
33. H. Jin fan, M. Knez, R. Scholz, K. Nielsch, E. Pippel, D. Hesse, M. Zacharias and U. Gosele, *Nat Mater*, 2006, **5**, 627-631.
34. H. J. Fan, M. Knez, R. Scholz, D. Hesse, K. Nielsch, M. Zacharias and U. Gösele, *Nano Letters*, 2007, **7**, 993-997.

35. Y. Yang, D. S. Kim, M. Knez, R. Scholz, A. Berger, E. Pippel, D. Hesse, U. Gosele and M. Zacharias, *J Phys Chem C*, 2008, **112**, 4068-4074.
36. J. P. Richters, T. Voss, D. S. Kim, R. Scholz and M. Zacharias, *Nanotechnology*, 2008, **19**, 305202.
37. M. Watanabe, M. Sakai, H. Shibata, C. Satou, S. Satou, T. Shibayama, H. Tampo, A. Yamada, K. Matsubara, K. Sakurai, S. Ishizuka, S. Niki, K. Maeda and I. Niikura, *Physica B: Condensed Matter*, 2006, **376-377**, 711-714.
38. C.-W. Fang, J.-M. Wu, L.-T. Lee, Y.-H. Hsien, S.-C. Lo and C.-H. Chen, *Thin Solid Films*, 2008, **517**, 1268-1273.

39. B. K. Meyer, H. Alves, D. M. Hofmann, W. Kriegseis, D. Forster, F. Bertram, J. Christen, A. Hoffmann, M. Straßburg, M. Dworzak, U. Haboeck and A. V. Rodina, *physica status solidi (b)*, 2004, **241**, 231-260.
40. H. P. He, H. P. Tang, Z. Z. Ye, L. P. Zhu, B. H. Zhao, L. Wang and X. H. Li, *Appl Phys Lett*, 2007, **90**, 023104.
41. T. B. Hur, Y. H. Hwang and H. K. Kim, *J Appl Phys*, 2004, **96**, 1507-1510.

Graphical Abstract

Manuscript title: Negative Thermal Quenching of Photoluminescence in Annealed ZnO/Al_2O_3 Core/Shell Nanorods

Authors: Yukun Wu, Junwen Li, Huaiyi Ding, Zhiwei Gao, Yiming Wu, Nan Pan, Xiaoping Wang*

Negative thermal quenching behavior of photoluminescence is observed in the annealed ZnO/Al_2O_3 core/shell nanorods, which is originated from the Al donor in ZnO induced through annealing process.